Protection mechanisms of the iron-plated armor of a deep-sea hydrothermal vent gastropod

Haimin Yao[a], Ming Dao[a], Timothy Imholt[b], Jamie Huang[a], Kevin Wheeler[a], Alejandro Bonilla[c], Subra Suresh[a], and Christine Ortiz[a,1]

[a]Department of Materials Science and Engineering, Massachusetts Institute of Technology, 77 Massachusetts Avenue, Cambridge, MA 02139; [b]Raytheon, Inc., 1001 Boston Post Road, Marlboro, MA 01752; and [c]Asylum Research, Inc., 6310 Hollister Avenue, Santa Barbara, CA 93117

Communicated by John D. Joannopoulos, Massachusetts Institute of Technology, Cambridge, MA, November 10, 2009 (received for review September 16, 2009)

Biological exoskeletons, in particular those with unusually robust and multifunctional properties, hold enormous potential for the development of improved load-bearing and protective engineering materials. Here, we report new materials and mechanical design principles of the iron-plated multilayered structure of the natural armor of *Crysomallon squamiferum*, a recently discovered gastropod mollusc from the Kairei Indian hydrothermal vent field, which is unlike any other known natural or synthetic engineered armor. We have determined through nanoscale experiments and computational simulations of a predatory attack that the specific combination of different materials, microstructures, interfacial geometries, gradation, and layering are advantageous for penetration resistance, energy dissipation, mitigation of fracture and crack arrest, reduction of back deflections, and resistance to bending and tensile loads. The structure-property-performance relationships described are expected to be of technological interest for a variety of civilian and defense applications.

exoskeleton | mollusc | biomechanics | nanomechanics | nanoindentation

Many organisms have evolved robust protective exterior structures over millions of years to maximize survivability in their specific environments. Biological exoskeletons or "natural armor" must fulfill various performance requirements such as wear resistance, dissolution prevention, thermal and hydration regulation, and accommodations for feeding, locomotion, and reproduction. Another critical function of these systems is mechanical protection from predators that can induce damage from, for example, penetration, fatigue, drilling, peeling, chipping, hammering, crushing, and kinetic attacks (1). Hence, a diverse array of macroscopic geometries, sizes, and hierarchical, multilayered composite structures exist (2). The shells of gastropod molluscs have long provided key insights into the mechanical performance of biological armor materials. Early on, Wainwright carried out macroscopic mechanical experiments on bivalve shells and formulated important questions on the contributions of different crystal textures to their strength and other functional properties (3). Soon after, Currey and Taylor characterized the properties of numerous mollusc shell microstructures and determined that the inner nacreous layer had superior mechanical properties (4). Subsequently, three decades of investigations ensued on nacre (5–9), leading to the generalized concept of "mechanical property amplification;" i.e., order of magnitude increases in strength and toughness exhibited by biological composites compared to their individual constituent materials beyond simple rule of mixture formulations (10–12). These discoveries engendered numerous efforts to produce nacre-mimetic composite materials that also exhibit mechanical property amplification (12–15). Design, inspired by nature, of engineering materials with robust and multifunctional mechanical properties [i.e., those which sustain a variety of loading conditions (16)] is a topic of major technological interest in a variety of civilian and defense applications (17).

Here, we identify the design principles of the shell of a gastropod mollusc from a deep-sea hydrothermal vent [order *Neomphalina* (18), family *Peltospiridae* (19), species *Crysomallon squamiferum* (20)]. This system has a trilayered structure unlike any other known mollusc or any other known natural armor, with a relatively thick compliant organic layer embedded between two stiffer mineralized layers, an outer iron sulfide–based layer and an inner calcified shell (Fig. 1*A*). High-resolution nanoscale testing methods, adapted from our prior work on other biological materials (21) were employed to quantify the local mechanical properties through the cross section of various layers. These results were then incorporated into a computational model of the entire multilayered exoskeletal structure in order to assess its penetration resistance under a simulated predatory attack. This process leads to the realization that each layer of the shell is responsible for distinct and multifunctional roles in mechanical protection. The overall methodology developed here involves direct correlation of the fine structure and properties to larger length scale biomechanical performance and function in the context of a common environmental threat (a predatory penetrating attack). The resulting mechanistic understanding has significant potential to expand current knowledge of the evolutionary design of functional structures in biology, as well as to inspire developments in protective layered design of engineered materials.

Trilayered Structure of the Shell of *C. squamiferum*

The majority of exoskeletal structures found in nature are multilayered composites with a diversity of layer thicknesses, layer sequences, number of layers, and nano- and microstructures employed for each layer (22–24), resulting in a distinctive "mechanical profile," i.e., spatial dependence of mechanical properties through the shell cross section specific to each species. A multilayered exoskeletal structure must sustain corresponding environmental threats, and its local mechanical profile is a critical determinant of the larger length scale biomechanical function including, for example, resistance to penetration, fracture modes, energy dissipation, elastic deformation, etc. Most gastropod molluscs have an outer cross-linked organic proteinaceous (conchiolin) periostracum that overlays a highly calcified (approximately 0.01–5 wt% organic) shell composed of sublayers of crystalline calcium carbonate (typically aragonite or calcite) of a variety of microstructures (2, 25). The shell of the gastropod mollusc studied here, *C. squamiferum* [recently discovered at the Kairei Indian hydrothermal vent field, Central Indian Ridge (18)], possesses a trilayered structure comprised of a mineralized iron sulfide–based outer layer (OL) containing greigite, Fe_3S_4 [verified by x-ray diffraction (XRD) and energy dispersive x-ray (EDX) spectroscopy (*SI Text*)], similar to its dermal sclerites (18, 26), up to 30 μm thick, followed by an organic middle layer (ML), presumably the periostracum, approximately 150 μm thick,

Author contributions: C.O., H.Y., M.D., T.I., A.B., and S.S. designed research; H.Y., M.D., J.H., K.W., and A.B. performed research; C.O., H.Y., M.D., T.I., A.B., and S.S. analyzed data; and C.O., H.Y., M.D., T.I., and S.S. wrote the paper.

The authors declare no conflict of interest.

Freely available online through the PNAS open access option.

[1]To whom correspondence should be addressed. E-mail: cortiz@mit.edu.

This article contains supporting information online at www.pnas.org/cgi/content/full/0912988107/DCSupplemental.

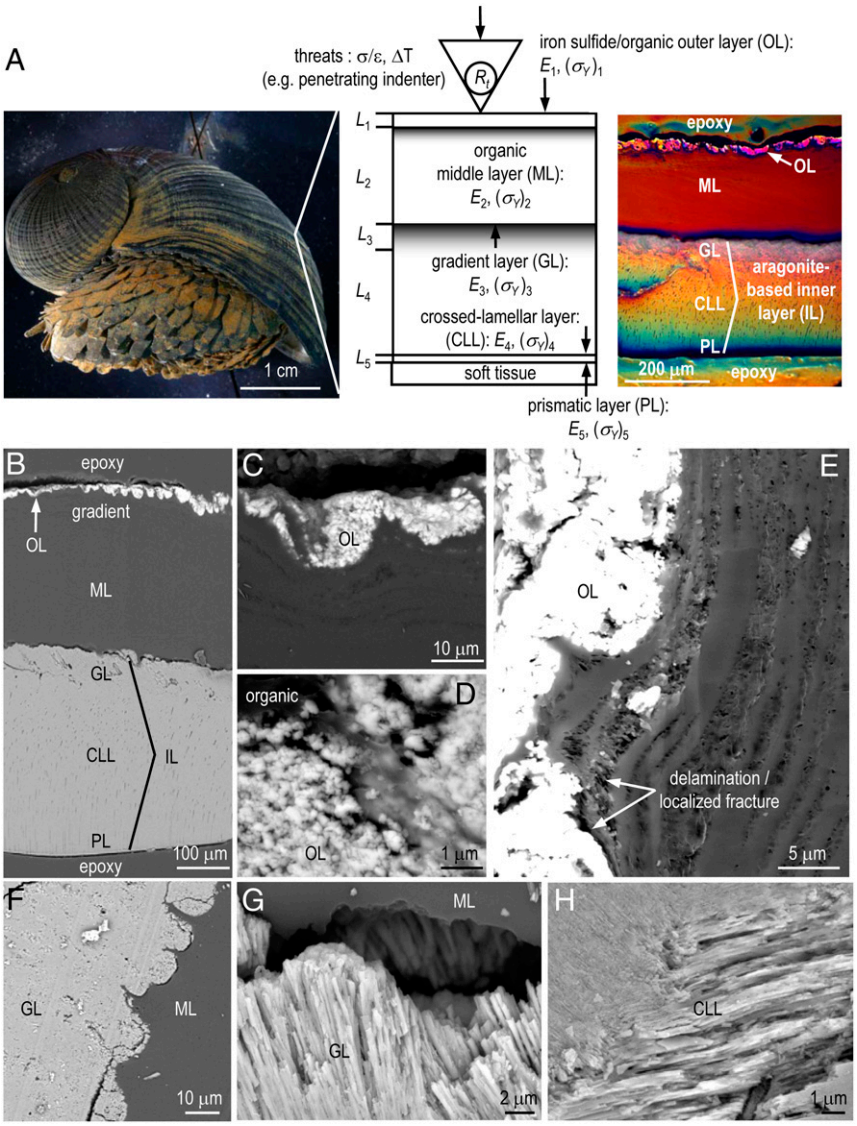

Fig. 1. Macroscopic and microscopic multilayered structure of the shell of *C. squamiferum*.. (*A*) Photograph of the entire snail showing geometry of shell (image taken and provided by Anders Warén) and optical micrograph with schematic of the cross section of the shell showing multilayered structure. (*B–H*) BSEM images of (*B*) entire shell cross section (contrast is reflective of mineral content), (*C*) interfacial geometry of outer and OL-ML gradient layer, (*D*) granular microstructure and intercalated organic in OL, (*E*) gradient interphase region between OL and ML, (*F*) interfacial geometry of ML and gradient IL, (*G*) interfacial microstructure of gradient IL, and (*H*) CLL.

followed by a transition to a highly calcified inner shell [inner layer (IL)] approximately 250 μm thick (Fig. 1*A* and *B*).

The OL exhibits a micro- to nanogranular composite structure composed of iron sulfide particles (down to approximately 20 nm diameter) and organic, and a heterogeneous "wavy" interfacial geometry resulting in nonuniform thickness (Fig. 1*C* and *D*). Previous studies (18, 26) on the purity and regularity of the iron sulfides suggest direct biological control by this gastropod, the only metazoan known to employ iron sulfide as a skeletal material (18). Between the OL and ML exists a gradient region (shown below via mechanical property measurement) with wavy rows rich in iron sulfide particles (Fig. 1*E*). The ML is exceedingly thick relative to the calcified IL, compared to typical periostraca (27). Other molluscs found in the same vicinity of the Kairei hot vent (28) also have thick periostraca relative to the calcified shell, for example, *Alviniconcha* (29), *Lepetodrilus* (30), and *Bathymodiolus* (31), while many other molluscs from hot vents at other geographical locations have thin periostraca (32). Periostraca are known to act as a template for shell mineralization and possibly serve as protection from harsh corrosive and dissolutive marine environments (e.g., brackish, cold-water, low-pH conditions), as well as chemical protection from boring secretions (27). We hypothesize that the periostracum may also be mechanically advantageous. The contribution of the periostracum to the mechanical performance of the entire exoskeletal structure is largely unknown, an effect that will be significant for thick periostraca, which we explore in this work and describe below. A similar wavy interfacial geometry is observed between the ML and calcified IL (Fig. 1*F*). The calcified IL is composed of aragonite (verified by XRD and EDX, see *SI Text*) and possesses a gradient layer (shown below via mechanical property measurement) with a typical crossed lamellar layer (CLL) microstructure (24) (approximately 50 μm thick, Fig. 1*G*), followed by a relatively thick layer also with a CLL microstructure (approximately 200 μm thick, Fig. 1*H*), followed by a thin prismatic layer (PL) on the inner surface of the shell (approximately 1.5 μm thick).

Nanoscale Mechanical Profile of the Shell of *C. squamiferum*

Instrumented nanoindentation (21, 33) (see *Materials and Methods*) in ambient conditions enables the quantification of

mechanical properties of the individual material layers of the *C. squamiferum* shell. Averaged values of the indentation stiffness calculated by the Oliver–Pharr (O-P) method (34), $E_{O\text{-}P}$, of the mechanically distinct OL, ML, and CLL were found to be 28.8, 8.0, and 98.9 GPa, respectively (Fig. 2*A*). A similar trend was observed for averaged values of the indentation hardness, $H_{O\text{-}P}$, which were determined to be 1.7, 0.5, and 5.4 GPa in the OL, ML, and CLL, respectively (Fig. 2*B*). This stiff (hard)–compliant (ductile)–stiff (hard) trilayer (Fig. 2*C*) is consistent with the known materials design described above, whereby a high degree of mineralization exists in the IL and OL and the absence of mineralization was observed in the ML. Similar trends were observed for experiments carried out in aqueous solution (phosphate buffered saline solution), albeit with reduction in magnitude of approximately 50% for the material property values. Simulations (described following) were carried out by using both sets of values (ambient and aqueous) and though ambient results are reported in detail, all trends reported were consistent for both sets of data. Previously reported values of the indentation modulus and hardness for the outer iron sulfide layer and organic conchiolin layer of the dermal sclerites were somewhat higher than those reported here, which could be due to differences in hydration, although the relative trends among layers were similar (26), which is the important focus of this work. Two gradient regions were observed; between the OL and ML (approximately 2.1 GPa/μm) and within the GL (approximately 1.8 GPa/μm) between the ML and CLL (Fig. 2*A* and *B*). The OL-ML gradient is likely due to the reduction in the concentration of iron sulfides from the OL to ML, which has been reported previously (26).

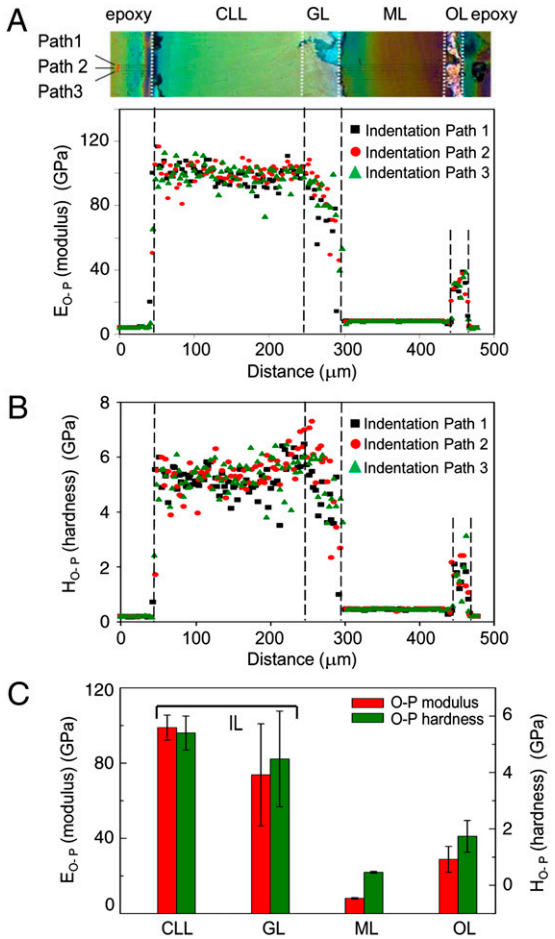

Fig. 2. Mechanical properties of the individual layers of the shell of *C. squamiferum*.. (*A*) Spatial distributions of O-P modulus and (*B*) hardness through the cross section (top optical microscopy image) for three different spatial pathways. (*C*) Pooled statistics (mean values and standard deviations) of O-P modulus and hardness for each layer.

Mechanisms of Energy Dissipation and Reduced Radial Displacement of the Shell of *C. squamiferum*

The experimentally measured local mechanical data were directly incorporated into a larger length scale computational (finite element) model representing the entire curved, multilayered shell structure (including the OL, ML, GL, and CLL) in response to a penetrating rigid indenter normal to the shell surface (Fig. 3*A*, see *Materials and Methods*). Modulus and yield stress values were obtained through elastic–perfectly plastic finite element fits to nanoindentation data, rather than the O-P data of Fig. 2. This model simulates the local loading of a common generic predatory attack (penetrating indent), for example, by Brachyuran crabs (*Austinograea sp.*) that were found in the same vicinity of the Kairei vent field as the gastropod (28). Crabs are known to compress gastropod mollusc shells between their chela (claws) (35), which is expected to result in a local indentation of the shell structure at the sites of the chela protruding "fingers." Each material layer was represented by an elastic–perfectly plastic constitutive model and maximum loads up to 60 N were employed, comparable in magnitude to the known crushing force generated by the chela of Brachyuran crabs (36). A complex multiaxial stress and strain field develops locally in response to the locally penetrating load (Fig. 3*B*). Plastic (inelastic) equivalent strain contours show that limited inelasticity occurs in the OL from high local stress concentrations at indenter tip (Fig. 3*B*, von Mises stress) while the bulk of inelastic deformation occurs in the

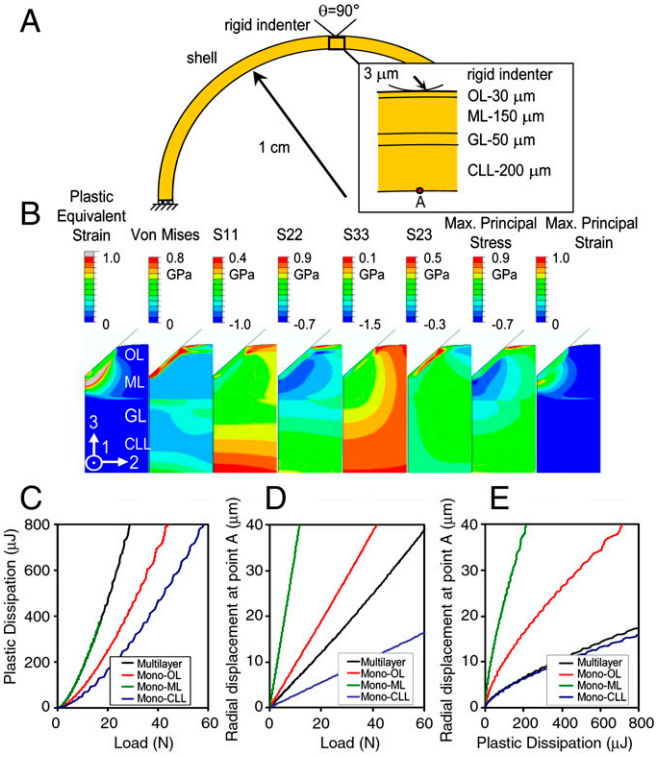

Fig. 3. Computational model of entire multilayered shell of *C. squamiferum*. (*A*) Finite element microindentation (indenter radius = 3 μm, included angle = 90°) simulation approximating the shell as hemispherical where the experimentally measured thickness and mechanical properties of the individual layers were taken into account. (*B*) Predicted stress and strain contours (maximum load, $F = 28$ N). Prediction of (*C*) plastic (inelastic) energy dissipation as a function of loading force and (*D*) radial displacement of point A on inner surface (see *A*) versus loading force and (*E*) radial displacement at point A versus plastic (inelastic) dissipation for the multilayered structure compared with three monolayered structures (Mono-OL, Mono-ML, and Mono-CLL).

underlying organic ML. The inelastic front arrests at the GL, thereby preventing yielding of the inner calcified shell layers.

The simulated indentation on the outer curved convex surface is observed to also induce bending of the entire exoskeletal structure near the point of loading. The rigid IL provides resistance to bending and radial displacements (discussed below in detail), as well as general structural support. Resistance to bending is also important for the "lip-peeling" mechanism of predation where, for larger molluscs that cannot be directly crushed by the chelae, the crab repeatedly inserts one of its chelae into the shell aperture and bends and breaks off a section of the thinnest outer lip until access to the internal body is gained (37). If the indentation load theoretically is sufficiently high in a penetrating attack to overcome the protection of the ML and to induce inelasticity of the IL through elevated tensile stresses (Fig. 3*B*, S_{11}, S_{22}, and S_{33}) due to bending, the IL would be susceptible to fracture normal to the shell surface. However, a number of "safety mechanisms" exist to mitigate catastrophic failure of the shell if this were to happen; propagating cracks from the IL are arrested by the highly inelastic ML (observed experimentally, discussed below). Moreover, a variety of energy dissipation mechanisms exist that are inherent to biological organic–inorganic hierarchical composite structures; for example, tortuous microcracking (6, 38) (observed experimentally, discussed below) which results in extension of intercalated organic material between mineralized constituents during their separation (5).

In order to further explore the mechanical advantages of the multilayered structure of the *C. squamiferum* shell, three hypothetical monolayered structures were generated by specifying the material properties in each simulation as those of OL, ML, and CLL, respectively, for comparison to the multilayered structure. Two functionally relevant parameters were tracked during the indentation: the plastic (inelastic) energy dissipation, which is a measure of the toughness of the entire exoskeletal structure, and the radial displacement of the inner surface of the shell at point A underneath the indenter tip (Fig 3*A*, *Inset*). The latter represents how much the inner soft tissues will be compressed during indentation (a potentially life-threatening blunt trauma situation). The increase in inelastic energy dissipation with loading force for the multilayered structure is approximately equivalent to that of the Mono-ML (Fig. 3*C*), consistent with the inelastic equivalent strain distributions (Fig. 3*B*) and much higher than those in Mono-OL and Mono-CLL. The increase in radial displacement at point A with loading force for the multilayered structure is much lower than in both Mono-ML and Mono-OL, but as expected, is larger than the stiff Mono-CLL (Fig. 3*D*). The radial displacement versus plastic (inelastic) dissipation (Fig. 3*E*) plot reveals that the multilayered system tracks the Mono-CLL closely, thereby achieving much reduced radial displacement simultaneously with large degrees of inelastic energy dissipation, both of which are beneficial for armor performance. The inherent curvature of the *C. squamiferum* shell plays a significant role in preventing radial displacements by increasing the stiffness of the shell structure while maintaining an equivalent level of inelastic energy dissipation, as well as reducing tensile stresses on the inner side of the shell. Simulations were repeated by using different indenter radii ranging up to 300 μm, and all trends presented were consistent within this range.

Mitigation of Inelasticity of the Inner Calcified Shell Layers of *C. squamiferum*

The monolayered CLL system is similar to many gastropod mollusc shells, which are highly calcified through the majority of their cross-sectional thickness (i.e., with relatively thin periostraca). In such shells, inelastic deformation takes place by extensive microfracture, and energy dissipation is achieved by the mechanisms mentioned previously due to the organic-inorganic nano- and microstructures, which undergo a variety of fracture processes (5, 6). Such mechanisms are particularly beneficial for resistance to fatigue cracking (the cumulative process of extending microcracks), which is known to take place via repeated compressive loading by crab chela (39). One primary advantage of the multilayered system of *C. squamiferum* is that inelasticity of the inner calcified layers are mitigated by the ML. Instead, an equivalent energy dissipation takes place via inelastic deformation of the unusually thick ML (Fig. 3*B* and *E*). There are a number of possible reasons that the avoidance of shell inelasticity and fracture as a protection mechanism might be advantageous to *C. squamiferum*; for example, it will further delay catastrophic fracture under fatigue loading. Localized fractures are expected to be more susceptible to dissolution at the low pH conditions of the hydrothermal vent (40).

Potential Role of the Iron Sulfide–Based Granular Coating to the Mechanical Performance of the Shell of *C. squamiferum*

The granular composite structure of the iron sulfide–based OL of the *C. squamiferum* shell is the first line of defense against a penetrating impact. Vickers microhardness experiments with the load applied perpendicular to the top surface of shell reveal interesting deformation mechanisms (Fig. 4*A*, maximum load approximately 9.8 N, maximum depth approximately 62 μm). Within the indent region, consolidation of the granular structure is observed within and around the indent. Localized microfractures exhibit tortuous, branched, and noncontinuous pathways, as well as jagged crack fronts resulting from separation of granules, all of which are beneficial for energy dissipation and preventing catastrophic brittle fracture. Such microfracture modes may serve as a sacrificial mechanism. Upon indentation, inelastic deformation will be localized in the softer organic material between the granule interfaces, which allows for intergranular displacement and friction (41) while simultaneously being compressed down into the softer ML. Shear of iron sulfide nanoparticles against the indenter surface is expected, in particular since penetrating attacks take place off-angle rather than directly on top of the shell apex (35), and can be facilitated by intergranular displacements during yielding of the OL. This provides a potential grinding abrasion and wear mechanism to deform and blunt the indenter (since biological penetrating threats are in reality deformable as well) that will continue throughout the entire indentation process. The local heterogeneous stress concentrations due to compression of the granules in the OL by the indenter are expected to further facilitate inelastic deformation of the indenter. Microhardness values are of the same or-

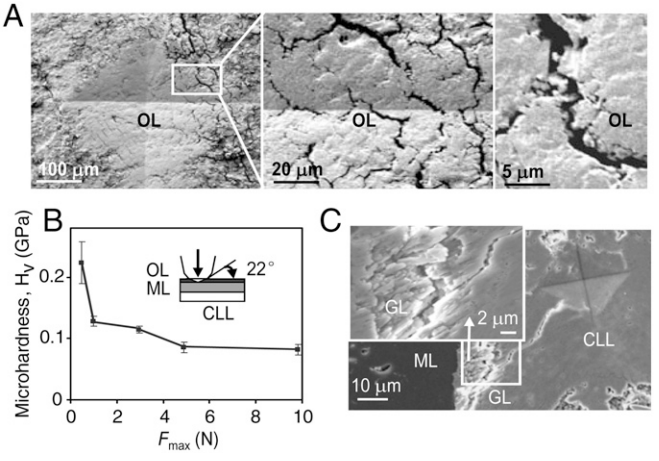

Fig. 4. Microindentation of the shell of *C. squamiferum*.. (*A*) SEM images of residual indents of Vickers microhardness experiments with load normal to the shell surface (maximum load approximately 9.8 N, depth 62 μm). (*B*) Measured Vickers hardness as a function of the maximum applied load (error bars indicate standard deviation). (*C*) SEM images of residual indent (load applied normal to cross section of GL). *Inset* shows the fracture processes in the GL.

der of the nanoscale hardness values for the ML and appear to be dominated by the organic component within and underneath the OL at increasing loads (Fig. 4*B*). Microhardness tests of the GL with the load applied perpendicular to the exoskeletal cross section show that cracks propagating through the IL do not continue into the ML (Fig. 4*C*); fracture was never observed in the highly inelastic ML via microhardness experiments at loads up to 10 N. Furthermore, the wavy geometry between the OL/ML results in heterogeneous interfacial stress distributions (*SI Text*) and a potential energy dissipating mechanism via interfacial delamination, which if inflated would subsequently be arrested by neighboring regions of interfacial compression and low shear, thereby preventing continuous and complete delamination of the entire OL from the ML or catastrophic fracture within the OL (42). It is interesting to see how *C. squamiferum* has created these additional different protection mechanism compared to other gastropod molluscs by using materials plentiful and specific to the deep-sea hydrothermal vent environment, i.e., vent fluids rich in dissolved sulfides and metals (18).

Multifunctional Biological Aspects of the Design of the Shell of *C. squamiferum*

The design principles of the trilayered shell of *C. squamiferum* (Fig. 5) exhibit many aspects that are different from the highly calcified shells of typical gastropod molluscs or any other natural armor. Each material layer serves distinct and multifunctional roles leading to many advantages (Fig. 5). The dermal sclerites of *C. squamiferum* also possess a similar iron sulfide–based OL and an inner organic ML on top of soft pedal tissue and, hence, no inner calcified layers exist as in the outer shell (18). The OL/ML covering the dermal sclerites is also expected to be beneficial for dissipating energy during kinetic projectile attacks of the radular teeth of the predatory Turrid gastropod *Phymorhynchus*, which was also found in the same vicinity of the Kairei vent field as *C. squamiferum* (18, 28). Similar cone snails are known to launch their radular teeth by targeting the foot and aperture of their prey rather than the shell, since calcified shells can easily resist their penetration (43). An inner calcified layer would not be as critical for the dermal sclerites since these structures would be able to sustain much larger displacements without jeopardizing the survivability of the mollusc. In addition to the mechanical advantages, the OL and ML were experimentally determined to resist low pH dissolution, and the ML was also predicted to be beneficial for protection against brief thermal impulses (*SI Text*). Hence, the shell of *C. squamiferum* is a multifunctional design providing protection against numerous environmental threats found in the deep-sea hydrothermal vent environment to maximize survivability. While *C. squamiferum* evolved relatively recently (18), the specific evolutionary origins of this mechanically robust shell have yet to be determined, i.e., it is unclear whether it represents an advanced functional adaptation as an antipredatory response or an exaptation (i.e., a trait that evolved to serve one function, but subsequently and simultaneously may serve other functions).

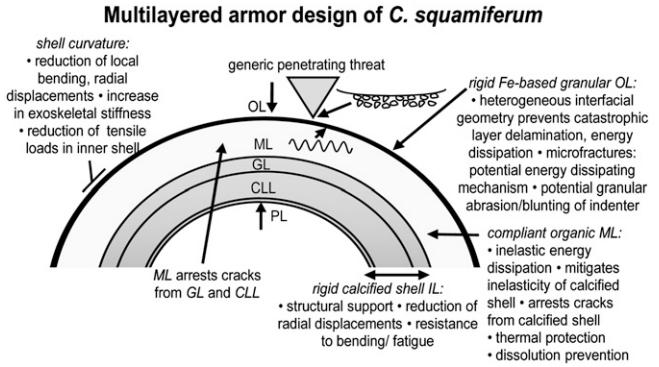

Fig. 5. Schematic of the multilayered design principles of the shell of *C. squamiferum*. Each material layer serves distinct functional roles leading to many advantages with regards to mechanical protection and penetration resistance.

Potential for Improved Biologically Inspired Engineering Applications

The design of synthetic bioinspired materials and structures that mimic natural systems is an enormous field with great potential for transforming numerous engineering and science fields, including civil engineering, bioengineering, mechanical engineering, materials science and engineering, chemical engineering, and aeronautics and astronautics (11). The design space for synthetic multilayered structural composites for protective applications is enormous, with a large number of potential design parameters, e.g., layer thickness, geometry, gradation, number, and sequence, anisotropic elastic constants, plastic anisotropy, strain-rate dependence, strain hardening/softening, delamination criteria, crush strength, interphase properties, spatial dependence of mechanical properties such as gradation, etc. Hence, predicting the response of such systems is extremely complicated and requires accurate information on the constituent material failure mechanisms, interactions and interfaces between constituent materials, the details of the penetration process, the rate- and length scale-dependent material constitutive laws of the material components, as well as the geometry and material properties of the penetrating object (44). Much of this information is typically unknown, and thus, frequently parametric approximation is necessary. Biological systems, such as the one described here, greatly reduce the engineering design space since efficient threat-protection design concepts have emerged through the lengthy evolutionary process that fulfill the necessary functions and constraints (17).

In particular, the efficient natural armor structural system described here sustains both mechanical loading, as well as thermal fluctuations with inherent mechanisms to prevent catastrophic failure. The multimaterial, trilayer design and advantageous curved geometry enables structural stiffening, reduction of radial displacements, penetration resistance, and stability during thermal impulses even with the presence of large mismatches between constituent materials. Trilayered sandwich composite designs have had limited use in military applications, and the concepts reported here could lead to bioinspired improvements and broader applicability and improved performance for human, vehicle, and structural armor. Additionally, the effects of layer geometry and material selection of different layers have been topics of considerable research concerning engineered materials optimized with sharp and graded layers for improved thermomechanical performance (45, 46) and indentation (47). The combination of material layering, compositional gradation, and microlayer and macroscopic geometrical design found in the gastropod mollusc shell offers important lessons for optimizing multifunctionality in engineering design aimed at enhancing mechanical performance characteristics and protection.

Furthermore, the numerous fundamental mechanical phenomena described here could also potentially be employed for use in protective engineering applications. For example, the amplification of energy dissipation through sacrificial "trapping" of tortuous noncatastrophic microcracks and localized nanoscale delamination of the outer granular Fe-based nanoparticle-organic composite layer (Fig. 3*E*). This concept of utilizing a sacrificial nanoparticle-organic coating to cause extensive energy dissipation through these mechanisms is largely unexplored in synthetic systems and could be utilized for any application requiring enhanced penetration resistance without the addition of excessive weight. Specific potential applications include synthetic engineered armor (e.g., human body, vehicle, and structural), automobiles (e.g., exterior paint of cars, motorcycles, etc.), construction applications

(e.g., pipelines that need resistance to rock penetration/abrasion), and sporting equipment (e.g., helmets, etc.). Such granular layers (GLs) may also hold potential for abrasion, blunting, and redirection of incoming threats. Lastly, another central issue to the field of engineered composites (e.g., aeronautics and astronautics), which has been considered at length, is the joining of different material layers together that are structurally stable and do not undergo complete delamination during loading. The heterogeneous layer-to-layer interfacial geometries described here also hold great potential for progress in this area.

Materials and Methods

Experimental. The shell of *C. squamiferum* was provided by Swedish Museum of Natural History. Samples were prepared by polishing and embedding in epoxy according to our previously reported protocols utilized for other biological materials (21). Backscattered electron microscopy images were taken with a JEOL JSM-6700F. EDX spectroscopy analysis was conducted with JEOL-5910 equipped with Röntec EDX system (Röntec GmbH, Germany) at an acceleration voltage of 15 kV. XRD analysis was conducted with Bruker D8 Multipurpose Diffractometer and Rigaku Rotating Anode X-Ray Powder Diffractometer. Nanoindentation experiments were carried out using a Triboindenter (Hysitron Inc.) in ambient conditions and with a molecular force probe indenter (Asylum Research, Inc.) in phophate-buffered saline solution with a cube corner diamond probe tip, accordingly to our previously reported protocols (21).

Finite Element Simulations. The *C. squamiferum* shell was modeled as a spherical (axisymmetric) multilayered structure with an inner radius taken as 1 cm (26), following our previous work (21). The thickness of the GL, CLL, ML,and OL were taken as 200, 50, 150, and 30 μm, respectively. Four-node bilinear axisymmetric quadrilateral element (CAX4R in ABAQUS) and four-node linear axisymmetric heat transfer quadrilateral element (DCAX4 in ABAQUS) are adopted in the simulations for mechanical and thermal resistance, respectively. The material properties of each layer were assumed homogeneous and modeled as isotropic elastic–perfectly plastic materials. The yield stress σ_y in each layer was deduced by using a FEA-based fitting technique developed in our previous works (33). To model the gradient, the CLL was divided further into 50 sublayers. The modulus and yield stress for each sublayer were obtained through linear interpolation from the values of GL and ML. Poisson's ratios of all materials were assumed equal to 0.3. A perfectly rigid indenter with a conical tip geometry with a 90° included angle and a 3 μm tip radius was employed as the penetrating indenter.

ACKNOWLEDGMENTS. We gratefully acknowledge Dr. Anders Warén of the Swedish Museum of Natural History in Stockholm for providing samples and image in Fig. 1*A*. We also acknowledge the MIT Nanomechanical Testing Laboratory for the experiments conducted here. We also gratefully acknowledge support of the National Science Foundation MIT Center for Materials Science and Engineering (DMR-0819762), the Advanced Materials for Micro and Nano Systems Programme and the Computational Systems Biology Programme of the Singapore-MIT Alliance, the US Army through the MIT Institute for Soldier Nanotechnologies (Contract DAAD-19-02-D0002), Raytheon, Inc., and the National Security Science and Engineering Faculty Fellowship (N00244–09–1–0064). M.D. and S.S. acknowledge partial support from the Interdisciplinary Research Group on Infectious Diseases, which is funded by the Singapore-MIT Alliance for Research and Technology. Discussions with Drs. Robert Jensen and Tusit Weerasooriya of the U.S. Army Research Laboratory were helpful during the course of this work.

1. Vermeij GJ (1993) *A Natural History of Shells* (Princeton Univ Press, Princeton, NJ).
2. Lowenstam HA, Weiner S (1989) *On Biomineralization* (Oxford Univ Press, New York).
3. Wainwright SA (1969) Stress and design in a bivalved mollusc shell. *Nature*, 224:777–779.
4. Currey JD, Taylor JD (1974) The mechanical behavior of some molluscan hard tissues. *J Zoo London*, 173:395–406.
5. Smith BL, et al. (1999) Molecular mechanistic origin of the toughness of natural adhesives, fibres and composites. *Nature*, 399:761–763.
6. Wang RZ, Suo Z, Evans AG, Yao N, Aksay IA (2001) Deformation mechanisms in nacre. *J Mater Res*, 16(9):2485–2493.
7. Bruet BJF, et al. (2005) Nanoscale morphology and indentation of individual nacre tablets from the gastropod mollusc *Trochus niloticus*. *J Mater Res*, 20(9):2400–2419.
8. Li X, Xu ZH, Wang R (2006) In situ observation of nanograin rotation and deformation in nacre. *Nano Lett*, 6(10):2301–2304.
9. Barthelat F, Li C-M, Comi C, Espinosa HD (2006) Mechanical properties of nacre constituents and their impact on mechanical performance. *J Mater Res*, 21(8):1977–1986.
10. Wegst UGK, Ashby MF (2004) The mechanical efficiency of natural materials. *Phil. Mag*, 84(21):2167–2181.
11. Ortiz C, Boyce MC (2008) Bioinspired structural materials. *Science*, 319(5866): 1053–1054.
12. Munch E, et al. (2008) Tough, bio-inspired hybrid materials. *Science*, 322:1516–1520.
13. Sellinger A, et al. (1998) Continuous self-assembly of organic-inorganic nanocomposite coatings that mimic nacre. *Nature*, 394(5907):256–260.
14. Bonderer LJ, Studart AR, Gauckler LJ (2008) Bio-inspired design and assembly of platelet reinforced polymer films. *Science*, 319(5866):1069–1072.
15. Podsiadlo P, et al. (2007) Ultrastrong and stiff layered polymer nanocomposites. *Science*, 318(5847):80–83.
16. Weiner S, Addadi L, Wagner D (2000) Materials design in biology. *Mater Sci Eng C*, 11:1–8.
17. Arciszewski T, Cornell J (2006) Bio-inspiration: Learning creative design principia. *Intelligent Computing in Engineering and Architecture*, ed Smith I (Springer, Berlin), pp 32–53.
18. Waren A, Bengtson S, Goffredi SK, Van Dover CL (2003) A hot-vent gastropod with iron sulfide dermal sclerites. *Science*, 302(5647):1007–1007.
19. Goffredi SK, Waren A, Orphan VJ, Van Dover CL, Vrijenhoek RC (2004) Novel forms of structural integration between microbes and a hydrothermal vent gastropod from the Indian Ocean. *Appl Environ Microb*, 70(5):3082–3090.
20. Takai K, Nakagawa S, Reysenbach A-L, Hoek J (2006) Microbial ecology of mid-ocean ridges and back-arc basins. *Geoph Monog*, 166:185–213.
21. Bruet B, Song J, Boyce MC, Ortiz C (2008) Materials design principles of ancient fish armor. *Nat Mater*, 7(9):748–756.
22. Uozumi S, Suzuki S (1981) The evolution of shell structures in the bivalvia. *Study of Molluscan Paleobiology*, ed Habe T (Kokusai Printing Press, Tokyo), pp 63–67.
23. Taylor JD, Kennedy WJ, Hall A (1969) The shell structure and mineralogy of the bivalvia: Introduction Nuculacea-Trigonacea. *Bull Brit Museum (Nat History) Zool*, 3:1–125.
24. Hedegaard C (1997) Shell structures of the recent Vetigastropoda. *J Mollus Stud*, 63:369–377.
25. Currey JD (1990) Biomechanics of mineralized skeletons. *Skeletal Biomineralization: Patterns, Processes and Evolutionary Trends*, ed Carter JG (Von Nostrand Reinhold, New York), pp 11–25.
26. Suzuki Y, et al. (2006) Sclerite formation in the hydrothermal vent "scaly-foot" gastropod—Possible control of iron sulfide biomineralization by the animal. *Earth Planet Sci Lett*, 242(1–2):39–50.
27. Harper EM (1997) The molluscan periostracum: An important constraint in bivalve evolution. *Palaeontology*, 40(1):71–97.
28. Van Dover CL (2002) Trophic relationships among invertebrates at the Kairei hydrothermal vent field (Central Indian Ridge). *Mar Biol*, 141:761–772.
29. Kiel S (2004) Shell structures of selected gastropods from hydrothermal vents and seeps. *Malacologia*, 46(1):169–183.
30. Hunt S (1992) Structure and composition of the shell of the archaeogastropod limpet *Lepetodrilus elevatus elevatus* (McLean, 1988). *Malacologia*, 34(1–3):129–141.
31. von Cosel R (2008) A new Bathymodioline mussel (bivalvia: Mytiloidea: Mytilidae: Bathymodiolinae) from vent sites near Kueishan Island, north east Taiwan. *Raffes Bull Zool*, 19(Supplement):105–114.
32. Waren A, Bouchet P (2001) Gastropoda and monoplacophora from hydrothermal vents and seeps: New taxa and records. *Veliger*, 44(2):116–231.
33. Tai K, Dao M, Palazoglu A, Suresh S, Ortiz C (2007) Nanoscale heterogeneity promotes energy dissipation in bone. *Nat Mater*, 6(6):454–462.
34. Oliver WC, Pharr GM (1992) An improved technique for determining hardness and elastic modulus using load and displacement sensing indentation experiments. *J Mater Res*, 7(6):1564–1583.
35. Williams MJ (1978) Opening of bivalve shells by the mud crab *Scylla serrata* forskal. *Aust J Mar Fresh Res*, 29:699–702.
36. Smith LD, Palmer AR (1994) Effects of manipulated diet on size and performance of Brachyuran crab claws. *Science*, 264(5159):710–712.
37. Kohn AJ (1999) Anti-predator defences of shelled gastropods. *Functional Morphology of the Invertebrate Skeleton*, ed Savazzi E (Wiley, New York), Chapter 14.
38. Kamat S, Su X, Ballarini R, Heuer AH (2000) Structural basis for the fracture toughness of the shell of the conch *Strombus gigas*. *Nature*, 405:1036–1040.
39. Boulding EG, Labarbera M (1986) Fatigue damage: Repeated loading enables crabs to open larger bivalves. *Biol Bull*, 171:538–547.
40. Van Dover CL, et al. (2001) Biogeography and ecological setting of Indian Ocean hydrothermal vents. *Science*, 294(5543):818–823.
41. Tai K, Ulm FJ, Ortiz C (2006) Nanogranular origins of the strength of bone. *Nano Lett*, 6(11):2520–2525.
42. Shimizu S, Macho GA (2007) Functional significance of the microstructural detail of the primate dentino-enamel junction: A possible example of exaptation. *J Hum Evol*, 52 (1):103–111.
43. Kohn AJ (2003) The feeding process in *Conus victoriae*. *The Marine Flora and Fauna of Dampier, Western Australia*, ed Wells FE (Western Australia Museum, Perth, Australia).
44. Cheeseman BA, Jensen R (2004) Protecting the future forces: Advanced materials and analysis enable robust composite armor. *AMPTIAC Quarterly*, 8(4):37–43.
45. Suresh S, Giannakopoulos AE, Olsson M (1994) Elastoplastic analysis of thermal cycling: Layered materials with sharp interfaces. *J Mech Phys Solids*, 42(6):979–1018.
46. Suresh S (2001) Graded materials for resistance to contact deformation and damage. *Science*, 292(5526):2447–2451.
47. Giannakopoulos AE, Suresh S (1997) Indentation of solids with gradients in elastic properties. Part I: Point force and part II: Axisymmetric indenters. *Int J Sol Struct*, 34(19):2357–2428.

Supporting Information

Yao et al. 10.1073/pnas.0912988107

SI Text

EDX. Spatially specific EDX data on the cross section of the *C. squamiferum* shell is provided in Fig. S1.

XRD. X-ray diffraction data on the shell of *C. squamiferum* is provided in Fig. S2.

Advantages of Heterogeneous Interfacial Geometries. Another interesting feature is the heterogeneous wavy interfacial geometry of the OL/ML, which was approximated in a modified multilayered finite element analysis (FEA) simulation and compared to a simulation containing a flat OL/ML interface. The wavy interfacial geometry did not have a significant effect on the overall inelastic energy dissipation, radial displacement, or bending stiffness of the entire exoskeletal structure; displacement of the indenter into the ML; or the local stress distributions in the underlying layers due to its small thickness in the overall geometry (Fig. S3). However, dramatically different discontinuous stress distributions were observed for the wavy interface within the OL itself and along the OL/ML interface compared to the flat OL/ML interface, with spatially distinct regions of high tensile and compressive normal stresses (S_{33}) and of high and low shear stress (S_{23}). Regions of high tensile S_{33} and high S_{23} provide susceptibility to interfacial delamination, which if initiated would subsequently be arrested by neighboring regions of interfacial compression and low shear (1). Localized interfacial delamination was, in fact, observed experimentally (Fig. 1*E*) at the OL/gradient interface, within the OL, and also within the iron sulfide–rich bands in the gradient region leading to the ML. This heterogeneous stress distribution therefore appears to provide an additional mechanism for energy dissipation in the most critical region of indentation via small localized regions of interfacial delamination while simultaneously preventing continuous and complete delamination of the entire OL from the ML or catastrophic fracture within the OL. The nanogranular substructure provides an even smaller level of waviness along the OL/ML, which results in advantageous smaller length scale heterogeneities in stresses and strains. It is interesting to see how *C. squamiferum* has created these additional different protection mechanism compared to other gastropod molluscs by using materials plentiful and specific to the deep-sea hydrothermal vent environment, i.e., vent fluids rich in dissolved sulfides and metals (2).

Thermal Simulations. *C. squamiferum* was found located at the base of the black smokers at the Kairei Field in a 1–2 m wide narrow transition zone where temperatures were measured in the range ≈2–10 °C (3). Deep sea hydrothermal vents are known to undergo drastic fluctuations in temperature due to emission of hot vent effluents (4). Hence, here we explore the resistance of the multilayered shell structure to a brief contact with a temperature of 100 °C (5). The thermal properties of OL, ML, CLL were taken as the values of greigite, that typical of organic biomacromolecules, and aragonite, respectively. A multilayered model (OL-ML-CLL, Fig. S4) was initially set to 2 °C. Then the outer surface was virtually heated up to 100 °C within 1 s, followed by a rapid cooling down to 2 °C within subsequent second (Fig. S4, dashed line). The maximum temperature on the inner surface (T_{inner}) in response to this transient pulse of extreme temperature was calculated to be 64 °C (Fig. S4). Interestingly, if the sequence of the ML and IL layers is reversed (OL-CLL-ML), a dramatic increase in T_{inner} is observed to 89.7 °C (Fig. S4) since the ML has higher thermal specific heat and lower thermal conductivity than the CLL. Placing the ML on the hotter side and IL on the colder side can enable the structure to exert maximum thermal protection. Lastly, a microlaminate structure approximating a nacreous microstructure was also simulated (Fig. S4) and, for this case, T_{inner} was observed to increase even further up to 91.7 °C. The apparent advantage of the multilayered structure of *C. squamiferum* over the microlaminate structure can be attributed to the high volume fraction of the organic phase characterized by low thermal conductivity and high heat capacity.

1. Shimizu S, Macho GA (2007) Functional significance of the microstructural detail of the primate dentino-enamel junction: A possible example of exaptation. *J Hum Evol*, 52(1):103–111.
2. Waren A, Bengtson S, Goffredi SK, Van Dover CL (2003) A hot-vent gastropod with iron sulfide dermal sclerites. *Science*, 302(5647):1007–1007.
3. Van Dover CL (2002) Trophic relationships among invertebrates at the Kairei hydrothermal vent field (Central Indian Ridge). *Mar Biol*, 141:761–772.
4. Van Dover CL, et al. (2001) Biogeography and ecological setting of Indian ocean hydrothermal vents. *Science*, 294:818–823.
5. McMullin ER, Bergquist DC, Fisher CR (2000) Metazoans in extreme environments: Adaptations of hydrothermal vent and hydrocarbon seep fauna. *Gravitational Space Biol Bull*, 13:13–23.

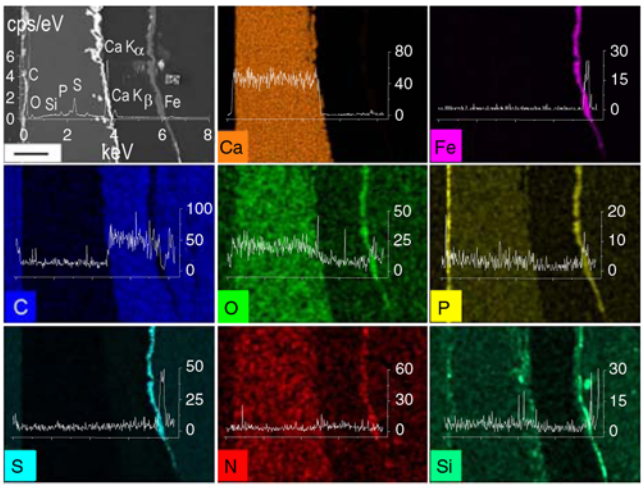

Fig. S1. EDX data on cross section of the *C. squamiferum* shell.

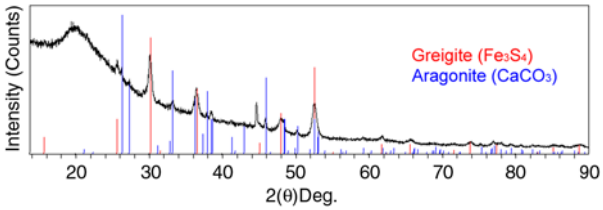

Fig. S2. X-ray diffraction of the *C. squamiferum* shell.

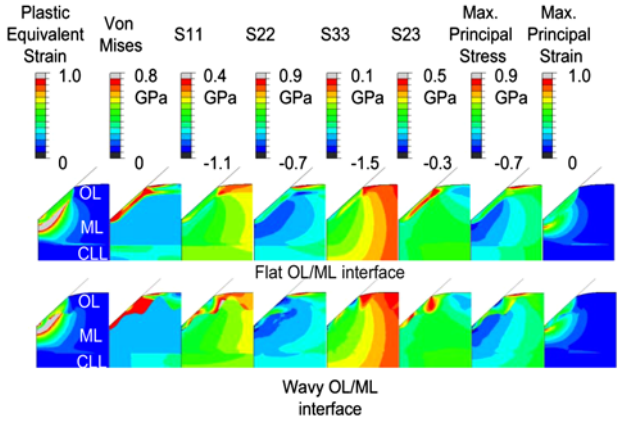

Fig. S3. Contours of predicted stress and strain for a wavy OL/ML interface compared to those for a flat OL/ML interface.

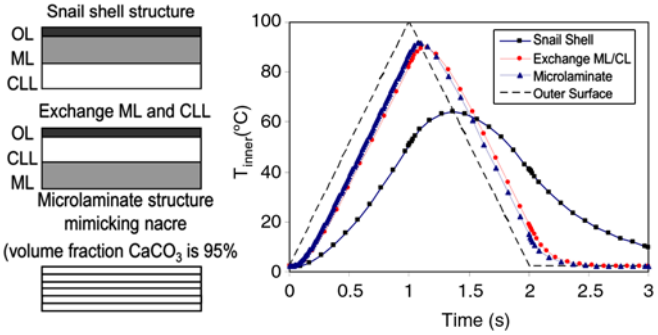

Fig. S4. Finite element simulation of resistance to thermal impulses of the *C. squamiferum* shell.